

Single-Chip CMOS Capacitive Sensor for Ubiquitous Dust Detection and Granulometry with Sub-micrometric Resolution

Marco Carminati^(✉), Pietro Ciccarella, Marco Sampietro,
and Giorgio Ferrari

Dipartimento di Elettronica, Informazione e Bioingegneria, Politecnico di
Milano, P.za Leonardo da Vinci 32, 20133 Milan, Italy
marco.l.carminati@polimi.it

Abstract. A monolithic CMOS chip able to count single airborne particles down to a diameter of 1 μm is presented. This mm-sized ASIC addresses the growing need for portable and miniaturized solid-state sensors monitoring air quality to be disseminated in the environment within pervasive wireless sensors networks. Particle counting and sizing are based on high-resolution capacitive detection. State-of-the-art performances (65 zF resolution with 40 Hz bandwidth) are enabled by the combination on the same chip of interdigitated microelectrodes (separated by 1 μm distance, matched with the particle size), and ultra-low-noise electronics connected to them achieving the lowest possible parasitic input capacitance. Chip design and characterization are illustrated.

1 Introduction

The relevance of the measurement of airborne particulate matter (PM) does not require extensive explanation. The adverse effects for the environment, the cultural heritage and the human health due to high concentrations of PM in the atmosphere have been abundantly demonstrated. Nevertheless, the strategies proposed and implemented so far, particularly in urban environments, such as vehicular traffic restrictions, have proved to be ineffective, mainly because of the complexity of such a multi-scale problem (involving the spatiotemporal variability of meteorological conditions and of emission sources and targets, from local street canyons to global levels). Dust suspension in the atmosphere is both due to natural phenomena (erosion, volcanic eruptions, and dust storms originated from the Sahara desert, considered the largest source of airborne dust in the world, producing about 70 millions of tons of dust per year transported by eastbound winds, 30% of which deposit in the eastern Mediterranean countries) as well as to anthropogenic sources, significantly varying from rural to urban areas.

Limiting only to the threats for health, they span from pathologies of the cardio-respiratory system to more subtle cell-level and gene-level interactions, which are object of wide on-going research [1]. The World Health Organization estimates that

in the year 2000 in Europe the average life expectancy loss due to exposure to $PM_{2.5}$ was 8.6 months, ranging from 3 months in Finland to 12–36 months in the Po valley [2]. Other reports account for 3 million deaths worldwide ascribable to $PM_{2.5}$ [3]. Regardless of the specific toxicological pathway, the risk due to the exposure to high concentrations of PM depends on the size and the chemical composition of the particles. Even particles of inert materials can be the carrier of dangerous pathogens. As illustrated in Fig. 1, the penetration inside the respiratory tract strongly depends on the particle diameter (for non-spherical particles, an equivalent aerodynamic diameter is defined). The distribution of the particles diameter is called *granulometric spectrum*. The smaller the diameter, the lower the filtering and the deeper is the penetration and the higher the risk of diffusion in the body and endocytosis inside the cells.

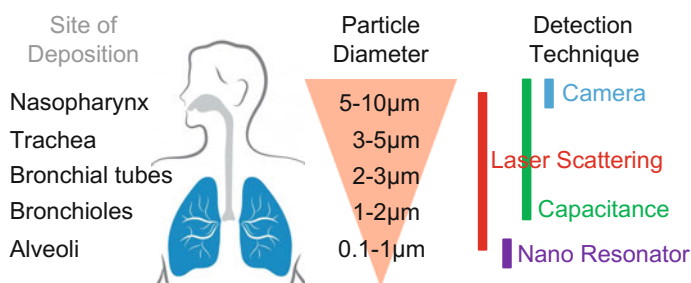


Fig. 1. Depth of PM penetration in the human respiratory system varying according to particle size and corresponding technologies allowing single-particle detection and granulometry

A broad range of instruments and techniques are currently employed for the characterization of PM, which can be analyzed either on-line (i.e. in the field) and off-line. The latter are mostly sophisticated laboratory techniques, based on the collection of PM on filters by means of samplers and impactors, often requiring preliminary sample preparation, such as metallization for electron microscopy or digestion for chemo-physical assays (such as elemental analysis by means of X-ray fluorescence spectroscopy [4]). On-line techniques comprise gravimetric accumulation and weighting, absorption of beta rays and laser scattering [5]. The latter, relying on the size-dependent intensity of the light pulse originated from the scattering of a laser beam focused on a stream of PM, is the only technique allowing single-particle analysis and granulometry. Unfortunately, the cost and bulkiness of these instruments prevent a massive deployment.

In the last years, several paradigm-shifting trends including smartphone-based participatory sensing [6], aimed at gaining a better insight in such a complex problem and mostly enabled by the fast development and pervasiveness of consumer-grade sensors, are emerging also in the environmental field. New interesting horizons are disclosed by wireless sensor networks. As summarized in Fig. 1, different emerging solutions based on solid-state miniaturized sensors, thus embeddable in low-cost and compact sensing nodes, but still allowing single-particle resolution, include CMOS

cameras with pixels of area comparable with larger PM, mass-sensitive MEMS and nano-resonators machined in silicon and micro-capacitance sensing [7].

2 Capacitive Dust Detection

In order to address the challenges described in the previous section, a non-optical technique based on the combination of microelectrodes and high-resolution capacitive sensing can be adopted [8]. As illustrated in Fig. 2, when a single particles enters the electric field between a pair of electrodes, the capacitance increases due to its larger dielectric constant with respect to air ($\epsilon_r = 1$). In order to maximize the sensitivity, the capacitor volume should be matched to the single particle size. For a parallel-plate geometry (facing electrodes of area A and distance d as in Fig. 2a), the capacitance value can be computed with the well-known expression (neglecting border effects):

$$C = \epsilon_0 \cdot \epsilon_r \cdot \frac{A}{d} \quad (1)$$

where ϵ_0 is the dielectric constant of vacuum and ϵ_r the relative dielectric constant of the material between the plates. With a spherical particle of radius r inside, the capacitance variation due to a change of a small volume fraction, can be estimated as:

$$\Delta C = \frac{4}{3} \cdot \pi \cdot \frac{r^3}{d^2} \cdot \Delta \epsilon_r \cdot \frac{\epsilon_0}{\epsilon_r} \quad (2)$$

where $\Delta \epsilon_r$ is the difference between the ϵ_r . As apparent from Eq. (2), the signal is increases with the dielectric contrast between the particle and the surrounding medium and by reducing the distance between the plates. If $\Delta \epsilon_r$ is known, it is also possible to estimate r from ΔC , clearly showing the potential for granulometry. Furthermore, the uncertainty in the estimation of an average ϵ_r (analogously to the average refractive index assumed in laser scattering) is mitigated by the fact that $r \sim \Delta \epsilon_r^{-1/3}$.

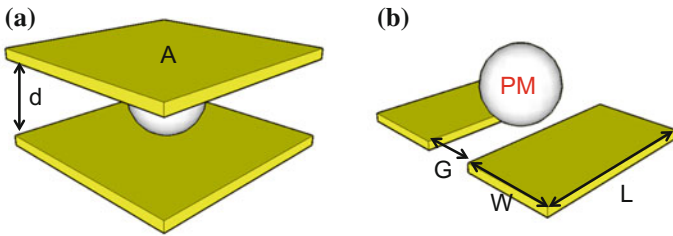


Fig. 2. Parallel-plate **a** and coplanar **b** microelectrodes configurations, both suitable for single particle capacitive detection when d and G are matched with the particle diameter

The advantage of this geometry the homogeneity of the electric field, allowing simple analytical expressions for the design. On the other hand, the major limit is the

risk of clogging when shrinking down d in the micrometric domain. A coplanar geometry (Fig. 2b) composed by a pair of electrodes (W by L) separated by a distance G , allows overcoming this risk, at the price of spatially inhomogeneous field that requires of the use of conformal mapping expressions [9] to estimate the capacitance:

$$C = 2\varepsilon_0 \cdot \frac{\varepsilon_r}{\pi} \cdot \ln \left[\left(1 + \frac{2W}{G} \right) + \sqrt{\left(1 + \frac{2W}{G} \right)^2 - 1} \right] \cdot L \quad (3)$$

Thanks to lithography, micrometric values for G can be easily achieved. A first proof-of-concept that capacitive detection of single micrometric airborne particles has been demonstrated with gold microelectrodes ($G = 4 \mu\text{m}$) patterned on glass and coupled with a low-noise amplifier realized with off-the-shelf discrete components [8]. The minimum resolution of this system was ~ 1 aF, resulting in a minimum detectable diameter of $\sim 7 \mu\text{m}$. In order to detect smaller particles, a single-chip solution has been developed, leveraging the combination of CMOS lithography and minimum stray capacitance at the input of the amplifier integrated on the same chip.

3 Design of a CMOS Monolithic PM₁ Detector

3.1 Electrodes and Architecture

The design starts from sizing the microelectrodes. The electrodes are fabricated on the topmost metal layer (metal 4 in the AMS 0.35 μm process here employed) and exposed to air by opening a window in the nitride passivation the same way used to expose bonding pads. Interestingly, this approach does not require any additional post processing of the chip that can be fabricated in any CMOS foundry and can be used as received. Under the electrodes no metal is present, in order to reduce the stray capacitance and the distance from the silicon substrate is 4 μm (Fig. 3a). An interdigitated geometry is chosen in order to cover uniformly the detection area. Finite-element numerical simulations (Fig. 3b) have been employed for optimal sizing of the electrodes. Targeting PM₁, W and G have been set to 1 μm , (slightly larger than the minimum 0.6 μm allowed by this technology for reliability considerations). With these dimensions, a sphere of 1 μm diameter (and minimum $\varepsilon_r = 2$) produces a capacitance change $\Delta C = 700$ zF.

Having set the electrode width and spacing, the second major choice concerns the total collection area and its partition into smaller “pixels”. From system level considerations, mostly related to the interfacing with proper fluidics forcing the collection of PM, the minimum detection area is set to 1 mm^2 . If this area were covered by a single couple of interdigitated electrodes, the total sensor capacitance would be 15 pF (with a stray capacitance to ground of about 3 pF). In these conditions, it would be impossible to detect the signal due to a single particle, being $\Delta C/C = 50$ ppb (corresponding to a dynamic range of 146 dB and an environmental stability better than 50 parts per billion). In order to reduce the dynamic range, allowing single particle resolution, two solutions have been adopted:

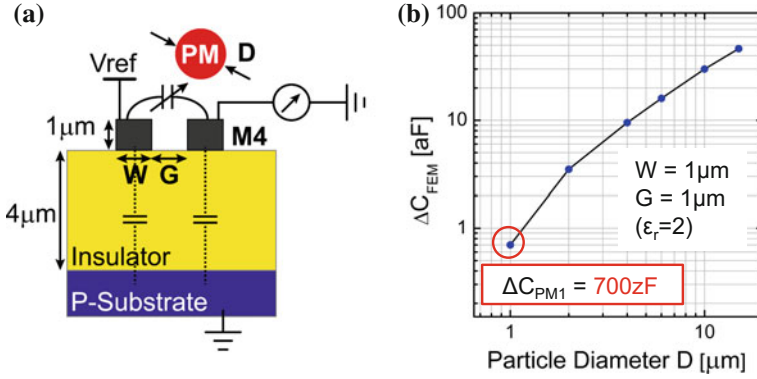


Fig. 3. **a** Cross-section of the CMOS PM sensor showing the capacitance-sensing electrodes fabricated in the highest metal level (M4) and exposed to air. **b** COMSOL simulations of the expected capacitance variation ΔC obtained when a single particle of diameter D deposits between these electrodes

- a *differential* architecture is chosen, so that only the differential signal is amplified by the chain when an unbalance is created by the deposition of a particle on one of the two combs. In order to avoid the risk that a large particles covering both couples produces a zero signal, the layout of the electrode has been arranged (Fig. 4) separating the positively-excited electrodes (+), from the negatively-excited electrodes (-). In one half of the array, the interdigitation is between (+) electrodes and the common input of the amplifier (virtual ground), while analogously, in the other half, the serpentine gaps separate (-) electrodes and the amplifier input. The symmetry is thus maintained and the two halves (C_{UP} and C_{DW}) are separated by a ground line. Furthermore, the differential configuration allows rejection of common mode disturbances (including thermal drifts) as well as the noise due to the voltage generator [10]. The only minor complication implied by this architecture is that the signal can be either positive or negative, depending on which half of the array the particle lands.
- the total sensing area has been *partitioned* in 32 slices of area $500\mu\text{m}$ by $70\mu\text{m}$. Correspondingly, the analog conditioning chains are replicated in 32 parallel channels. The pixel area corresponds to an input capacitance smaller than 0.5pF , suitable for achieving excellent noise performance.

The whole architecture of the readout circuit is shown in Fig. 4. It consists of 32 identical channels including the electrodes and the conditioning chain, which comprises the amplification stages, the square-wave multiplier (synchronous with the square-wave stimulation of the electrodes at 100–500 kHz, biased alternatively at V_{REF} and GND, as commonly performed to read half-bridge differential capacitive sensors such as in inertial MEMS [11]) and a g_m -C low-pass filter with a selectable bandwidth (40, 85, 360, 750 Hz) completing the *lock-in* block.

A sensor bandwidth of 85 Hz per channel is enough to correctly sample single deposition events considering typical PM concentrations (max ~ 50 particles/liter for

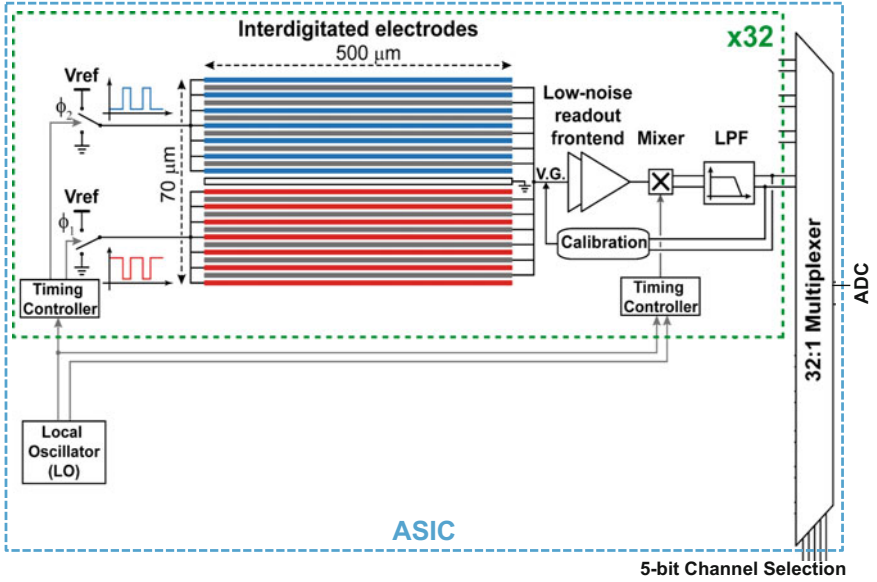


Fig. 4. Architecture of the electronics: each of the 32 channels comprises two sets of interdigitated differential electrodes and a low-noise signal conditioning chain

PM_{10}) and sampling flow-rates (\sim liter/min), with a very low coincidence probability, giving a total data rate of ~ 3 kSa/s. Given such a relatively slow rate of information to be processed, the chip is connected to an external ADC with a single output by means of a 32:1 multiplexer (MUX) controlled by 5 parallel bits. It should be noted that the low-pass filter must be placed before the MUX (thus requiring 32 filters instead of a single one and, unfortunately, much more silicon area) in order to avoid the long settling time required by a single filter which should update its voltage after each switching of the MUX (and would be limiting the scanning frequency to ~ 1.6 Hz in the case of the narrowest bandwidth).

3.2 Front-End

Given the capacitive nature of the sensor, the optimal choice for the front-end amplifier is a transimpedance stage with capacitive feedback (Fig. 5). This allows frequency-independent gain and minimum noise [12]. The size of the input transistors is set in order to match the amplifier input capacitance with the sensor capacitance, in order to achieve minimum noise. The feedback capacitance C_F of the first stage is set equal to 20 fF. A transistor in feedback operating in sub-threshold regime handles the input DC leakage current. A second stage with a similar topology and high gain (40) is cascaded in order to reduce the impact of the g_m -C filter.

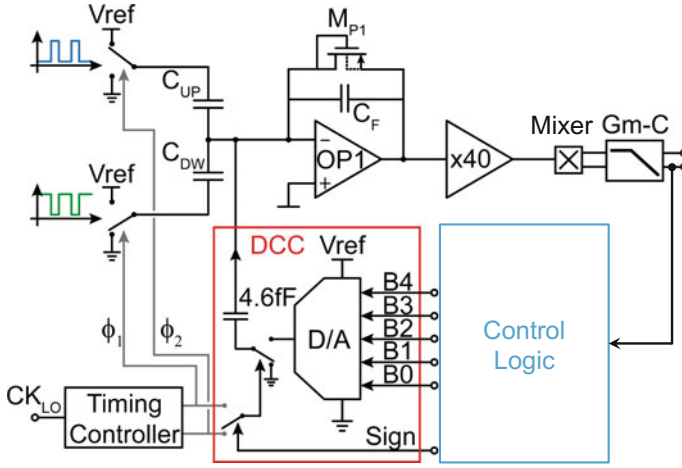


Fig. 5. Scheme of the analog amplification chain

In order to compensate the mismatch between the two pairs of electrodes, an automatic auto-zeroing network has been also implemented. It is composed by a Digital-to-Capacitance Converter (DCC) and a control logic. The DCC comprises a fixed compensation capacitor of 4.6 fF connected at the chain input and driven by a 5-bit resistive DAC featuring a LSB = 150 aF and measured DNL of 15 aF. Finally, a current-subtracting network allows reducing the noise at low frequency by a factor 4.

4 Experimental Results

The fabricated prototype is shown in Fig. 6. The total chip area is 2.5 mm by 2.4 mm and current consumption is 25 mA (at 3.3 V power supply) [13]. The bonding pads are located on one side, in order to leave the other sides free from bonding wires for easier coupling the chip with proper fluidics. After the functional tests confirmed the circuit performances, such as amplifier bandwidth (10 kHz–2 MHz) and noise (65 zF at 40 Hz) are in agreement with the simulations, the chip has been validated with the real-time deposition of single particles.

Consistently with the previous experiments with the discrete-component setup, mineral talc (abundant, nontoxic, with an average diameter of 8 μm and $\epsilon_r = 2.4$) is employed. Talc powder was suspended in air by means of a properly-driven vibrating loudspeaker, placed in the same Faraday cage. Before starting the experiments, microphotographs of the electrodes surface are taken. Then the speaker is activated and, when a channel displays a capacitance step, the experiment is stopped and another photograph of that channel is taken, in order to correlate the measured ΔC with a microscope image of the deposited particle. By adjusting the concentration of talc loaded on the loudspeaker and its distance from the detector, it is possible to easily achieve the condition of single depositions with rates of a few events per minute. Fixed defects or previously deposited particles act as reference points, useful when comparing images taken in different moments.

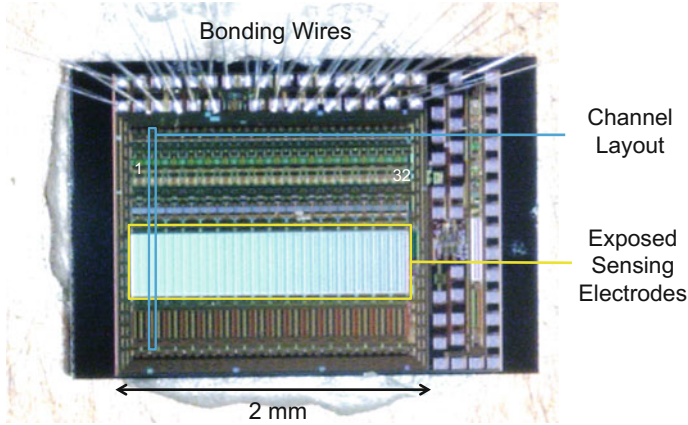


Fig. 6. Chip microphotographs: 32 parallel channels are visible, the sensing area is 1.15 mm^2

A typical deposition event is shown in Fig. 7: the capacitance recording (sampled with a temporal resolution better than 100 ms) shows a clear jump of 1 aF, due to the deposition of a single talc particle with a diameter of about $1.5 \text{ }\mu\text{m}$, extracted from the microscope image. Despite the uncertainties in the estimation of the equivalent diameter of non-spherical particles from bidimensional microscope image, good agreement is observed between the measured jumps, the imaged particles and the simulation of Fig. 3b. Thanks to the measured noise floor of 65 zF, a $1 \text{ }\mu\text{m}$ particle (giving a $\Delta C = 700 \text{ zF}$ for the minimum ϵ_r) is detected with a SNR $>20 \text{ dB}$.

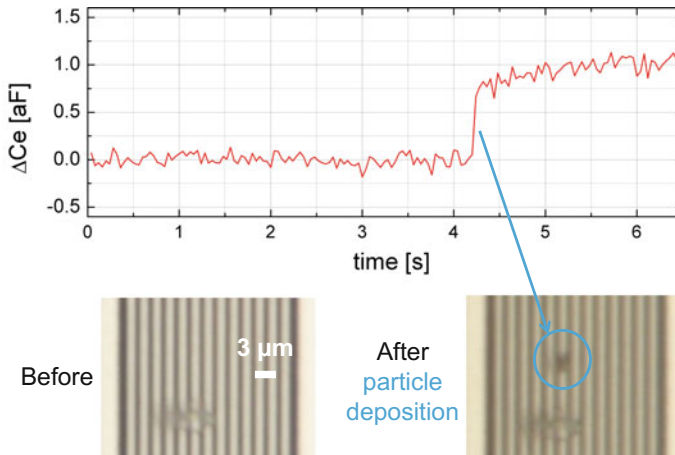


Fig. 7. Real-time capacitive tracking of the deposition on the interdigitated electrodes of a single dust particle ($\epsilon_r = 2.4$) of $1.5 \text{ }\mu\text{m}$ diameter producing a capacitance increase of 1 aF

Figure 8 reports several deposition events, corresponding to two dust clouds, showing the operation of the acquisition system (based on the acquisition board NI PCI-6289 controlled by a custom LabView program) in multichannel tracking.

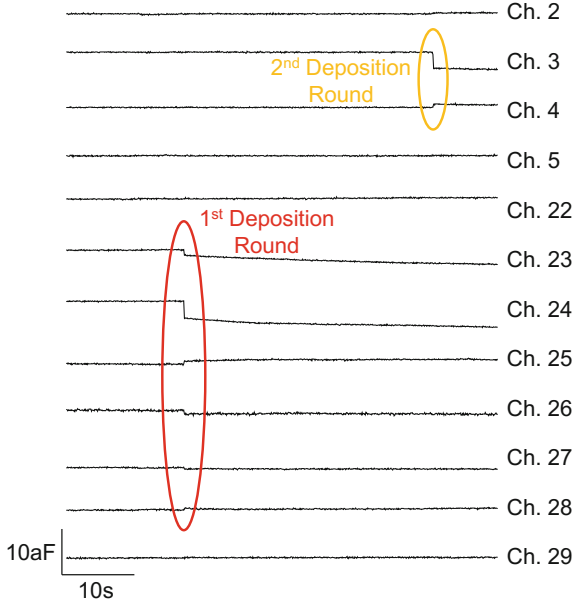


Fig. 8. Multichannel tracking of several PM particles depositing from talc clouds in two rounds

5 Conclusions

The first single-chip CMOS sensor for counting and granulometry of particles in the 20–1 μm range has been presented, illustrating the key design aspects required to achieve deep sub-attoFarad resolution (and improving by more than two orders of magnitude what achieved with discrete components).

Conductive particles do not represent a sever risk of shorting thanks to the insulating layer constituted by the thin native aluminum oxide that naturally forms on the exposed electrodes. Instead, humidity in the form of water droplets can produce large artifacts and false counts (due to the large $\epsilon_r = 80$ of water). To prevent this issue, analogously to laser-scattering instruments, heated probes can be employed, as well as on-chip heaters or proper layout of the hottest power dissipating areas on chip.

Thanks to the abrupt change in capacitance produced by the PM deposition, slow drifts (due for instance to temperature drifts which, in any case, are mitigated by the differential architecture) do not prevent detection on long measuring times.

Finally, for the deployment in the environment in a pervasive and ubiquitous ways, the micro-system should be completed with:

1. a particles concentration and capture system. For instance, electric fields, fluidodynamic impactors or thermophoretic forces could be combined with this CMOS platform for enhanced low-concentration operation.
2. a surface cleaning system for periodical removal of deposited PM and restoring of the initial condition for long term operation (based for instance of vibrating mechanical energy or local air jets). The low cost of silicon for large production volumes, allows also considering alternative employment scenarios including disposable cartridges.

The feasibility of the capacitive technique has been demonstrated down to PM_1 and the detector has been optimized from the point of view of noise. Further engineering is clearly required: power dissipation, electrode geometry, total detection area and number of channels can be tuned and adapted to the final application of the chip, spanning from fixed urban nodes, to portable dosimeters or even embedment inside consumer devices such as smartphones.

References

1. G. Sancini et al., Health risk assessment for air pollutants: alterations in lung and cardiac gene expression in mice exposed to Milano winter fine particulate matter ($PM_{2.5}$). *PLoS ONE* **9**, 109685 (2014)
2. WHO (2006) Air quality guidelines—global update 2005
3. S.S. Lin et al., A comparative risk assessment of burden of disease and injury attributable to 67 risk factors and risk factor clusters in 21 regions, 1990–2010: a systematic analysis for the global burden of disease study 2010. *Lancet* **380**, 2224 (2012)
4. A. Zacco et al., Analysis of settled dust with X-ray fluorescence for exposure assessment of metals in the province of Brescia, Italy. *J. Environ. Monitoring* **11**, 1579 (2009)
5. A. Chung, D.P.Y. Chang, M.J. Kleeman, K.D. Perry, T.A. Cahill, D. Dutcher, E.M. McDougall, K. Stroud, Comparison of real-time instruments used to monitor airborne particulate matter. *J. Air Waste Manage. Assoc.* **51**, 109 (2001)
6. E.G. Snyder et al., The changing paradigm of air pollution monitoring. *Environ. Sci. Tech.* **47**, 11369 (2013)
7. M. Carminati, G. Ferrari, M. Sampietro, Emerging miniaturized technologies for airborne particulate matter pervasive monitoring. *Measurement* (in press)
8. M. Carminati, L. Pedalà, E. Bianchi, F. Nason, G. Dubini, L. Cortelezzi, G. Ferrari, M. Sampietro, Capacitive detection of micrometric airborne particulate matter for solid-state personal air quality monitors. *Sens. Actuators A* **219**, 80 (2014)
9. J.Z. Chen, A.A. Darhuber, S.M. Troian, S. Wagner, Capacitive sensing of droplets for microfluidic devices based on thermocapillary actuation. *Lab Chip* **4**, 473 (2004)
10. M. Carminati, G. Gervasoni, M. Sampietro, G. Ferrari, Note: differential configurations for the mitigation of slow fluctuations limiting the resolution of digital lock-in amplifiers. *Rev. Sci. Instrum.* **87**, 026102 (2016)
11. J. Wu, G.K. Fedder, L.R. Carley, A low-noise low-offset capacitive sensing amplifier for a $50\text{-}\mu\text{g}/\sqrt{\text{Hz}}$ monolithic CMOS MEMS accelerometer. *IEEE J. Solid-State Circ.* **39**, 722 (2004)

12. M. Crescentini, M. Bennati, M. Carminati, M. Tartagni, Noise limits of CMOS current interfaces for biosensors: a review. *IEEE Trans. Biomed. Circ. Syst.* **8**, 278 (2014)
13. P. Ciccarella, M. Carminati, M. Sampietro, G. Ferrari, Multichannel 65 zF rms resolution CMOS monolithic capacitive sensor for counting single micrometer-sized airborne particles on chip. *IEEE J. Solid-State Circ.* (submitted)

Sensors

Proceedings of the Third National Conference on
Sensors, February 23-25, 2016, Rome, Italy

Andò, B.; Baldini, F.; Di Natale, C.; Marrazza, G.;
Siciliano, P. (Eds.)

2018, XII, 429 p. 258 illus., Hardcover

ISBN: 978-3-319-55076-3